10796 *Biochemistry* **2010,** *49,* 10796–10802
DOI: 10.1021/bi101743w

BIOCHEMISTRY
including biophysical chemistry & molecular biology
Article

Stability and Membrane Orientation of the Fukutin Transmembrane Domain: A Combined Multiscale Molecular Dynamics and Circular Dichroism Study[†]

Daniel A. Holdbrook,[‡] Yuk Ming Leung,[‡] Thomas J. Piggot,[‡] Phedra Marius,[§] Philip T. F. Williamson,*[,§] and Syma Khalid*[,‡]

[‡]*School of Chemistry, University of Southampton, Highfield, Southampton SO17 1BJ, U.K., and* [§]*School of Biological Sciences, University of Southampton, Highfield, Southampton SO17 1BJ, U.K.*

Received July 2, 2010; Revised Manuscript Received November 23, 2010

ABSTRACT: The N-terminal domain of fukutin-I has been implicated in the localization of the protein in the endoplasmic reticulum and Golgi Apparatus. It has been proposed to mediate this through its interaction with the thinner lipid bilayers found in these compartments. Here we have employed multiscale molecular dynamics simulations and circular dichroism spectroscopy to explore the structure, stability, and orientation of the short 36-residue N-terminus of fukutin-I (FK1TMD) in lipids with differing tail lengths. Our results show that FK1TMD adopts a stable helical conformation in phosphatidylcholine lipids when oriented with its principal axis perpendicular to the bilayer plane. The stability of the helix is largely insensitive to the lipid tail length, preventing hydrophobic mismatch by virtue of its mobility and ability to tilt within the lipid bilayers. This suggests that changes in FK1TMD tilt in response to bilayer properties may be implicated in the regulation of its trafficking. Coarse-grained simulations of the complex Golgi membrane suggest the N-terminal domain may induce the formation of microdomains in the surrounding membrane through its preferential interaction with 1,2-dipalmitoyl-*sn*-glycero-3-phosphatidylinositol 4,5-bisphosphate lipids.

Recently, a number of genes that are implicated in the O-linked glycosylation of α-dystroglycan (αDG),[1] a vital component of the dystrophin-associated complex that anchors muscle fibres to the extracellular scaffold, have been identified (*1*). These genes include *fukutin-I* (*fk1*), *fukutin related protein* (*FKRP*), *LARGE*, *POMGnT1*, *POMT1*, and *POMT2*. Mutations in these genes have been shown to lead to the aberrant glycosylation of αDG, resulting in a broad spectrum of congenital muscular dystrophies. Analysis of these genes suggests that they encode type II membrane proteins with putative glycosyltransferase activity, consistent with the hypoglycosylation of the αDG observed in patients carrying mutations in these genes (*1*). A number of studies have since demonstrated that these proteins are located in the ER/Golgi Apparatus (GA) complex, consistent with their proposed role in the glycosylation of αDG (*2*−*5*). Interestingly, a number of mutations identified in these genes result in the mislocalization of the protein within the cell, suggesting that their retention within the ER/GA complex is vital for the appropriate glycosylation of αDG (*3*).

Protein retention within the ER/GA complex is a highly dynamic process that relies crucially on the regulation of both antero- and retro-grade transport steps (*6*). A number of bioinformatic and biochemical studies have demonstrated that retrograde transport is largely regulated by receptor-mediated recognition of specific extra-membranous motifs on ER/GA resident proteins (*7*). In contrast, anterograde transport appears to be dependent on the shorter transmembrane domain that is typically found in ER/GA resident proteins (*7*, *8*). Indeed, the N-terminal transmembrane domains of FK1 and FKRP have been shown to be sufficient for retaining the protein within the GA (*9*). It has been suggested that the retention of ER/GA resident proteins may be mediated through the interaction of these shortened transmembrane domains and the distinctive lipid composition found in the ER/GA membranes. Although the role of the N-terminal TMDs in the retention of these proteins within the ER/GA complex is clear, we are far from a molecular description of this process, and at present, several models based on lipid-mediated protein sorting and protein oligomerization have been proposed (*6*, *8*, *10*, *11*).

To begin to investigate the role that the bilayer composition within the ER/GA complex may play in the retention of these proteins, we have undertaken a combined molecular dynamics (MD) and circular dichroism (CD) study of the transmembrane domain of the protein encoded by *fukutin* over a range of bilayer compositions to ascertain how the protein responds to differing bilayer thicknesses. We focus on FK1TMD, a short fragment composed of the first 36 N-terminal residues of fukutin, which is thought to insert into the membrane of the Golgi Apparatus. While the structure of FK1TMD has not been resolved, preliminary CD studies indicated a mostly α-helical structure under conditions that mimic the lipid bilayer (*12*).

[†]P.M. and P.T.F.W. are funded by a Wellcome Trust Fellowship to P. T.F.W. S.K. is an RCUK fellow. T.J.P. is funded by BBSRC.

*To whom correspondence should be addressed. P.T.F.W.: e-mail, p.t.williamson@soton.ac.uk; phone, +44 (0) 2380 594350. S.K.: e-mail, s.khalid@soton.ac.uk; phone, +44(0) 2380 59476; fax, +44 (0)23 8059 3781.

[1]Abbreviations: αDG, α-dystroglycan; ER, endoplasmic reticulum; FK1TMD, fukutin transmembrane domain; GA, Golgi Apparatus; MD, molecular dynamics; ATMD, atomistic molecular dynamics; CGMD, coarse-grained molecular dynamics; CD, circular dichroism; CHOL, cholesterol; PIP2, 1,2-dipalmitoyl-*sn*-glycero-3-phosphatidylinositol 4,5-bisphosphate; DHPC, 1,2-dihexanoyl-*sn*-glycero-3-phosphocholine; DDPC, 1,2-didecanoyl-*sn*-glycero-3-phosphocholine; DLPC, dilauroylphosphatidylcholine; DMPC, dimyristoylphosphatidylcholine; DPPC, dipalmitoylphosphatidylcholine; POPC, palmitoyloleoylphosphatidylcholine; POPS, palmitoyloleoylphosphatidylserine; PE, phosphatidylethanolamine; PS, phosphatidylserine; IP3, inositol 1,4,5-trisphosphate; SM, sphingomyelin; MLV, multilamellar vesicle; SUV, small unilamellar vesicle.

 Published on Web 11/24/2010

METHODS

Atomistic molecular dynamics (ATMD) simulations of FK1TMD (modeled as an idealized α-helix) were conducted in (i) water, (ii) 1 M NaCl, (iii) a dimyristoylphosphatidylcholine (DMPC) bilayer, and (iv) a dipalmitoylphosphatidylcholine (DPPC) bilayer. The insertion of FK1TMD into (i) dilauroylphosphatidylcholine (DLPC) (ii) DPPC, (iii) POPC, (iv) POPS, and (v) mixed lipid bilayers was studied via coarse-grained molecular dynamics (CGMD) simulations.

Generation of the FK1TMD Model. We created a model of the 36-residue transmembrane domain of fukutin (FK1TMD) by threading the FK1TMD sequence to an idealized α-helix using Modeller 9v7 (*13*). The resulting helix was evaluated for stereochemical integrity using Procheck (*14*). This model was used for all of the atomistic simulations and also for creating the coarse-grained version of FK1TMD.

Details of Atomistic Simulations. Atomistic simulations were performed using GROMACS 4.0.7 (www.gromacs.org) (*15*−*17*). The simulations used an extended united atom version of the GROMOS96 force field (*18*). Berger parameters were used for phospholipids, as described in ref *19*. Water molecules were treated explicitly using the SPC water model (*20*). Sodium and chloride ions were used to neutralize the charge of the simulation systems. All lipid and protein bonds were constrained using the LINCS algorithm (*21*), and water molecules were constrained using the SETTLE algorithm (*22*), allowing a time step of 2 fs to be used. The velocity rescaling thermostat, with a time constant for coupling of 0.1 ps, was used to maintain the system temperature (*23*). The Berendsen barostat, with a time constant of 1.0 ps, was used to maintain the system pressure at 1.0 bar (*24*). Electrostatic interactions used a cutoff of 1.0 nm, with interactions beyond this cutoff treated using the smooth particle mesh Ewald (PME) method (*25*). The van der Waals interactions also used a cutoff of 1.0 nm with a long-range dispersion correction applied for the energy and pressure. The neighbor list was updated every 10 steps. The system components of each simulation are summarized in Table I of the Supporting Information. All simulations were run for 50 ns. The conformational properties of FK1TMD were analyzed using GROMACS tools and DSSP (*26*). Visualization was conducted with VMD (*27*).

Details of Coarse-Grained Simulations. All CG simulations were performed using GROMACS 4.0.7 (www.gromacs.org) (*15*−*17*) with the MARTINI CG force fields. All simulations involved self-assembly of a lipid bilayer in the presence of one FK1TMD molecule from a random configuration of protein, lipids, ions, and water as described in refs (*28*−*30*). The CG parameters for DPPC, DLPC, POPC, ions, and water molecules are given in ref *28*. The parameters for the 1,2-dipalmitoyl-*sn*-glycero-3-phosphatidylinositol 4,5-bisphosphate (PIP2) lipid headgroup were derived through matching the bond and angle distributions from a CG inositol 1,4,5-trisphosphate (IP3) (*31*) simulation to atomistic simulations of IP3 performed using the GROMOS carbohydrate parameters (*32*). The remainder of the PIP2 lipid parameters were the same as those used for the CG DPPC lipid. Parameters for amino acids are given in refs *29*, *33*, and *34*. The integrity of the FK1TMD helix was retained by implementing an elastic network model as described in ref *33*. For simulations of FK1TMD in the more complex Golgi Apparatus membrane, we used the MARTINI2.0 force field because of the greater range of lipid models available (*35*). The complex GA membrane was composed of 50% PC, 20% phosphatidylethanolamine (PE), 12% PIP2, 8% phosphatidylserine (PS), and 10% sphingomyelin (SM). All phospholipids had palmitoyl fatty acid tails in both the *sn*-1 and *sn*-2 positions of the glycerol backbone. The ratio of phospholipid to cholesterol was 16:1 (0.16). This composition is similar to that of the GA (*36*). As with the atomistic simulations, analyses of the CG simulations were performed using GROMACS tools and locally written code, and visualization was conducted with VMD (*27*).

Details of Circular Dichroism Experiments. The hydrophobic peptide FK1TMD (MQRINKNVVL ALLTLTSSAF LLFQLYYYKH YLSARN) was synthesized by Peptide Protein Research Ltd. to more than 50% purity. DHPC (C6:0), DDPC (C10:0), DLPC (C12:0), DMPC (C14:0), and DPPC (C16:0) were purchased from Avanti Polar Lipids. Sodium phosphate was obtained from Sigma.

For lipids with chain lengths of more than 10 carbons, we reconstituted the FK1TMD peptide into unilamellar vesicles by dissolving the peptide and lipid at a molar ratio of 100:1 in methanol. This was dried to a thin film by vacuum evaporation. Multilamellar vesicles (MLVs) were formed by hydration and agitation in 5 mM sodium phosphate buffer (pH 7.4). MLVs were sonicated to clarity to form small unilamellar vesicles (SUVs). The final concentration of FK1TMD in the CD samples was 0.2 mg/mL as determined by its absorbance at 280 nm (E_{280} = 5960 M^{-1} cm^{-1}). For DHPC (C6:0), the samples were prepared in an identical manner, resulting in the reconstitution of FK1TMD into DHPC micelles.

The CD spectrum of the FK1TMD peptide reconstituted in unilamellar vesicles composed of saturated phospholipids of varying chain lengths was measured using a Jasco J720 spectropolarimeter fitted with a heater and a 1 mm path length quartz cuvette (Hellma) at 25 and 43 °C. The spectrum scan was performed from 300 to 190 nm using a spectral bandwidth of 2 nm, a scanning speed of 100 nm/min, and a response time of 4 s. Six spectra were recorded and averaged for subsequent analysis. CD spectra were analyzed between 195 and 240 nm to determine the secondary structure composition of FK1TMD in the different lipid environments using the CONTIN/LL analysis algorithm (*37*, *38*) provided on the Dichroweb CD analysis server (*39*, *40*). The analysis was performed using basis set 7 that has been widely used to study secondary structural elements of membrane peptides and surface-associated proteins.

RESULTS

Atomistic Simulations. Initially, the stability of the FK1TMD model was assessed in an aqueous environment. The protein lost much of its α-helical structure within the first 10 ns of simulation; by the end of the 50 ns simulation, only residues V8−L13 and L25−H30 were in an α-helical conformation (see Figures 1 and 2 of the Supporting Information).

Next, the stability of the FK1TMD model in the vicinity of a membrane-mimetic phospholipid bilayer was investigated. Simulations were initiated with the FK1TMD model in two positions relative to the phospholipid bilayer (i) in the water region just above the phospholipid headgroups of a DMPC bilayer and (ii) in a TM orientation, in which the principal axis of the α-helix was perpendicular to the bilayer plane. As expected given the in vivo environment of the ER/GA membranes, the secondary structure of the model was more stable near a phospholipid bilayer compared to that in just a water/ion environment. When initially positioned in the aqueous phase just above the lipid headgroups,

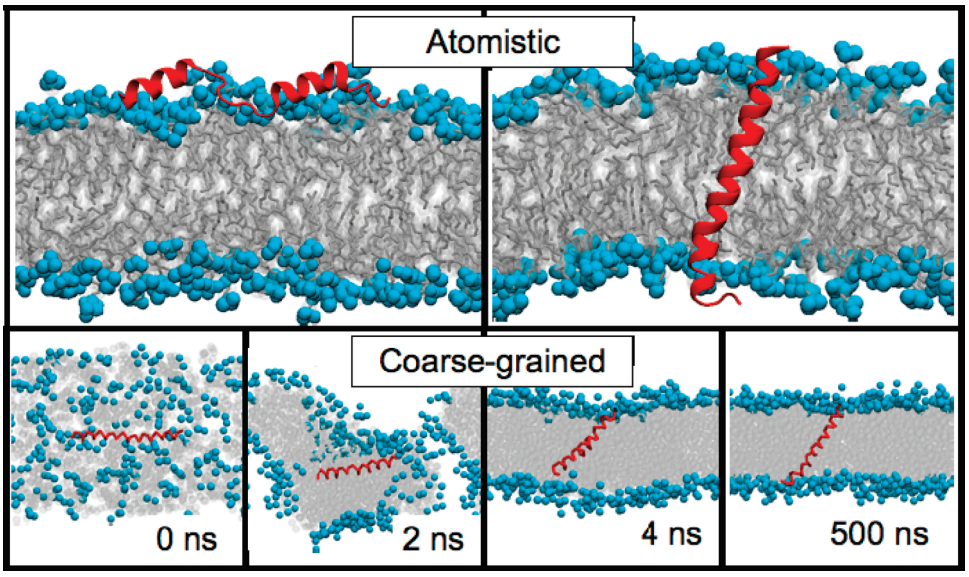

FIGURE 1: Final snapshots from ATMD after 50 ns in DMPC (top) and DPPC bilayer self-assembly and protein insertion from CGMD (bottom). Lipid headgroups are colored cyan and the tails gray, and FK1TMD is colored red. Water and ions have been omitted for the sake of clarity.

FK1TMD retained its α-helical structure in two short regions at either end of the peptide (Figure 1). The region between these two α-helices (L13−F20) became unstructured (see Figure 3 of the Supporting Information). When manually positioned perpendicular to the bilayer plane, the helix generally remained in a stable α-helical conformation (between R3 and H30), although some unfolding was observed at the C-terminal end (Y31−N36) (see Figure 1 and Figures 4 and 5 of the Supporting Information). To assess the effect of the bilayer thickness on the stability of FK1TMD, we also simulated the helix in a DPPC lipid bilayer. DPPC has longer tails than DMPC, and thus a thicker hydrophobic core region. The pattern of unfolding at the C-terminal end observed in the DMPC simulations was reproduced in the DPPC simulations. Structural drift of the helix was measured by calculating the mean root-mean-square deviation (rmsd) of the backbone Cα atoms from the starting structure over the last 25 ns of each simulation. The rmsd values were similar in both lipid environments, 0.33 ± 0.04 nm in DMPC compared to 0.28 ± 0.02 nm in DPPC (see Figure 6 of the Supporting Information).

Coarse-Grained Simulations. CGMD, in which four heavy atoms are replaced with a single, spherical particle, to reduce the complexity of the system enables longer time scales to be studied. This has permitted the study of bilayer self-assembly and the insertion of peptides into lipid bilayers (*29*, *30*, *41*). The preferred membrane localization and orientation of FK1TMD has been investigated using CGMD. The FK1TMD model was constrained to an idealized α-helix by using an elastic network. The 1 μs simulations were initiated from a random arrangement of lipids, peptide, water, and counterions to allow the self-assembly of the bilayer and unbiased insertion of the protein. The effect of the bilayer thickness on the orientation of FK1TMD was assessed by simulating the model in DLPC (three particles in both tails), DPPC (four particles in both tails), and POPC (four particles in one tail and five in one tail) phospholipids. In all the CG simulations, the bilayer self-assembly proceeded via the stalk formation mechanism as previously reported for DPPC lipids from comparable CGMD studies (*28*, *29*). FK1TMD adopted a TM orientation within the membrane, with the axis of the α-helix oriented approximately perpendicular to the plane of the bilayer (Figure 1). FK1TMD was occasionally oriented parallel to the plane of the bilayer at the start of the simulations, particularly in DLPC lipids. However, after a short period of time (~75 ns), one end of the helix inserted into the bilayer followed by the rest of the helix, such that it was traversing the bilayer. It retained this TM orientation for the remainder of the simulation, although its precise tilt with respect to the bilayer plane was observed to fluctuate. The tilt angle of FK1TMD calculated during the final 100 ns of the CG simulations was $39 \pm 11°$ in DLPC and $30 \pm 9°$ in DPPC. Presumably, the greater average tilt angle in the shorter DLPC lipid tails is a result of matching the hydrophobic region of the protein with the lipid tails. To further investigate the possibility of the lipid tail length influencing the FK1TMD tilt angle, we ran an additional set of CG simulations, this time with POPC phospholipids. PO tails are longer than DP and DL tails (the POPC CG lipid model implemented within MARTINI has five particles for the oleoyl tail and four particles for the palmitoyl tail, compared to the four particles for each palmitoyl tail in DPPC) and also contain an unsaturated bond (oleoyl group), which gives the tails a characteristic "kink". In agreement with the trend observed in our DPPC and DLPC simulations of a smaller tilt angle in longer lipid tails, the mean tilt angle of FK1TMD calculated during the final 100 ns of the CG simulations was $17.6 \pm 7°$ (see Figure 7 of the Supporting Information).

A conserved N-terminal motif, R/K-x-x-R/K, has been shown to be required for the correct localization of some glycotransferases within the GA (*3*). The R/K-x-x-R/K motif of FK1TMD (R-I-N-K) is located between residues R3 and K6. To investigate the role of this motif in the membrane localization and orientation of FK1TMD, we calculated the number of contacts (contact defined as an interatomic distance of ≤6 Å) between the protein and the phospholipid headgroup particles by sampling the last 100 ns of the 1 μs CGMD trajectories at 0.4 ns intervals. Full details of the protein−lipid contacts are provided in the Supporting Information. In all three lipid bilayers (DLPC, DPPC, and POPC), the N-terminal residues between M1 and N7 made regular contacts with the phospholipid headgroup particles. In particular, R3 and K6 had a strong propensity to interact with lipid headgroup particles; together, they accounted for >20% of all headgroup−protein contacts in simulations of all three lipid bilayers (see Tables 2−4 of the Supporting Information). Presumably,

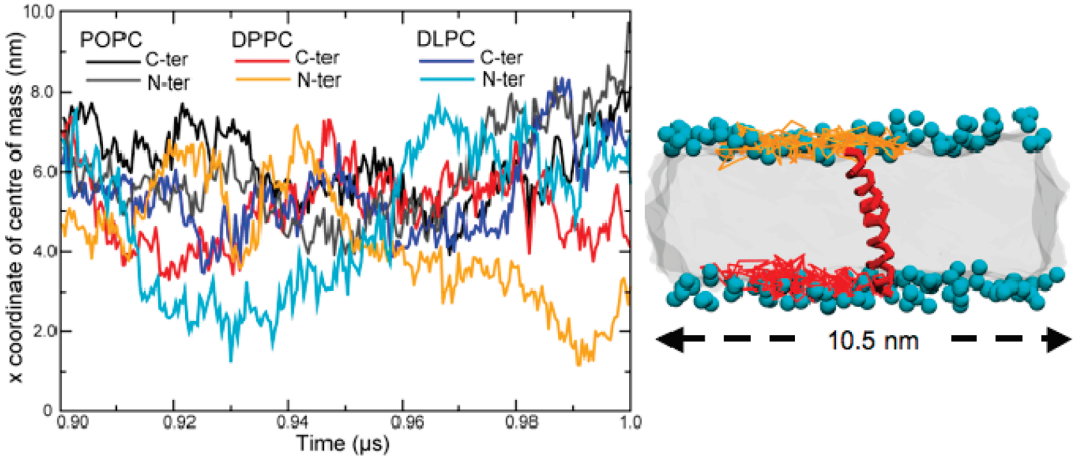

FIGURE 2: Center of mass movement of terminal residues of FK1TMD in POPC, DPPC, and DLPC lipids (left) and cartoon representation of the same movement in DPPC (right). The bars indicate the maximum and minimum values (x dimension). Lipid phosphate particles are colored cyan, and the tails are represented as a gray surface. The movement of the N-terminal residue is colored in orange, while the C-terminal movement is colored red.

these charged residues serve to anchor the N-terminal end of the α-helix in the headgroup region of the zwitterionic lipid bilayer.

At the C-terminal end, residues Y28−N36 made regular contacts with the lipid headgroup particles. In particular, residues K29, R35, and N36 had a marked propensity to interact with the lipid headgroups; together, they make up ∼15% of the total headgroup−protein contacts in the DLPC simulations and ∼20% in the DPPC and POPC simulations. These observations suggest that the charged residues at both N- and C-terminal ends of the helix play a key role in anchoring the protein in a TM orientation in the lipid bilayer. The fluctuations in the tilt angles suggest that there may be a degree of mismatch between the width of the hydrophobic patch on FK1TMD and the hydrophobic region of the bilayer defined by the lipid tails. In addition to the protein−lipid contacts, we also measured the protein lateral motion by monitoring the position of the center of mass of the terminal residues in the $x-y$ plane during the last 100 ns of the simulations (Figure 2). The helix exhibited a high degree of lateral mobility. In all three lipids, the lateral movement of the helix in the $x-y$ plane was up to ∼7 nm in either the x or y dimension.

In Vivo Environment of FK1TMD. the GA membrane is composed of a complex mixture of lipids, including anionic lipid headgroups. Having established the influence of the lipid tail length on FK1TMD orientation and mobility, we then investigated any potential affinity of the protein for particular lipid headgroups, in particular the influence of the anionic lipids. First, we performed self-assembly simulations of FK1TMD in POPS lipids. Although the high charge density of a 100% POPS bilayer does not reflect the in vivo environment of FK1TMD, these simulations were useful in determining the effect of anionic lipid headgroups, as we could compare directly with our simulations of FK1TMD in POPC. Changing the headgroups in our simulations had the largest effect on the protein tilt angle. We observed an increase in the tilt angle from 17.6 ± 7° in POPC to 25.5 ± 9° in POPS. This is presumably driven by the interaction of R3 and K6 in the N-terminus and K29 in the C-terminus with the POPS headgroup atoms (see Table 5 of the Supporting Information). The lateral mobility of the protein in the two different lipid types was similar. To investigate the effect of the different headgroups in an environment more representative of the GA membrane, we simulated a more complex bilayer. This consisted of a mixture of DPPC, DPPE, PIP2, SM, and DPPS lipids in a 50:20:12:10:8 ratio and also cholesterol (CHOL) at a 16:1 phospholipid:cholesterol ratio (*36*).

In the complex GA membrane, R3 and K6 at the N-terminus of FK1TMD made a large number of contacts with the headgroups of all lipid types. These two positively charged amino acids made the most contacts with the highly negatively charged PIP2. Indeed, the interactions of PIP2 with R3 and K6 accounted for 12% of the total contacts between FK1TMD and the phospholipid headgroups. In contrast, the interactions of PIP2 with K29 and R35, at the C-terminus of the FK1TMD, accounted for only 5% of the total headgroup contacts. The hydroxyl group of CHOL makes the most contacts with a discrete region between I4 and L10 at the N-terminus of FK1TMD. This region accounted for approximately 55% of the total contacts between CHOL and FK1TMD. Conversely, CHOL makes fewer and more diffuse contacts with the C-terminal amino acids. The interactions of SM with FK1TMD followed the same trends as those with DPPC. While the tilt angle of FK1TMD in the more complex GA membrane was 23.6 ± 8°, this is intermediate between the tilts observed for the DPPC/DLPC and POPC bilayers but similar to the tilt angle of 25.5° measured from our simulations of FK1TMD in pure POPS.

To evaluate the distribution of the system components, we calculated density profiles of FK1TMD and the various lipid headgroups (Figure 3). The distribution indicates similar positions of the DPPC, DPPE, and DPPS lipids with respect to the bilayer normal, which would be expected for lipids with the same tail groups. The SM lipids are placed slightly farther apart; i.e., they are displaced slightly toward the aqueous phase. This appears to be a result of lipid−lipid contacts within the bilayer. The shorter CHOL moieties are located closer to the hydrophobic core of the bilayer. The slight asymmetry in the CHOL density is a result of one molecule flipping into the opposite leaflet during the equilibration procedure. Visual inspection of the simulation trajectories revealed a clustering of PIP2 lipids around the N-terminus of the FK1TMD (Figure 3). To further investigate this clustering, the radial distribution was calculated for the glycerol-linked phosphates of PIP2 relative to the K6 and K29 residues of FK1TMD (Figure 8 of the Supporting Information). The distributions show that PIP2 is found more often in the proximity (within 1 nm) of K6 than in the proximity of K29. In comparison to PIP2, the radial distribution of the DPPE

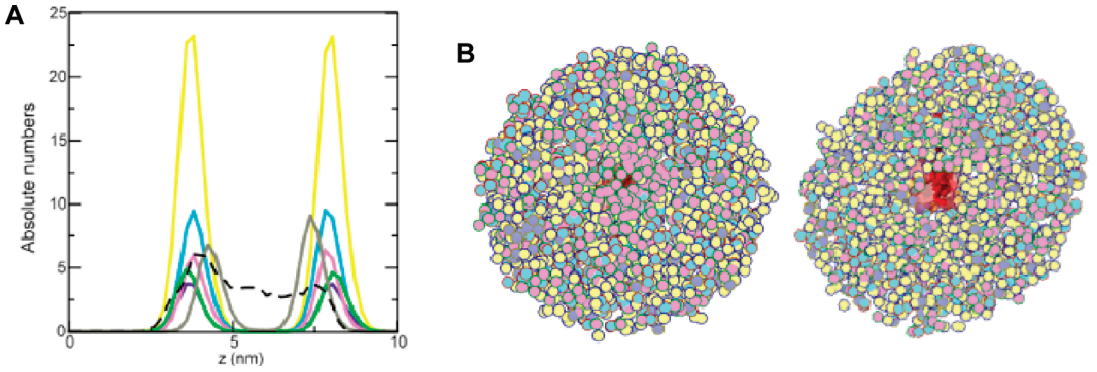

FIGURE 3: (A) Density of protein and lipid headgroup particles along the *z* dimension. The curves representing the different lipids are colored as follows: yellow for DPPC, cyan for DPPE, violet for DPPS, magenta for PIP2, green for sphingomyelin, gray for CHOL. The black dashed line represents data for FK1TMD. (B) Lipid headgroup particles within 3 nm of the R and K residues of the N-terminus (left) and C-terminus (right) (colors as in panel A; cholesterol and sphingomyelin have been omitted for the sake of clarity, and FK1TMD is colored red). The trajectory is fitted on the protein using a least-squares procedure, and the frames are superimposed at 40 ns intervals over the 1.5 μs trajectory. Clustering of the PIP2 lipids near the N-terminus is evident. Such clustering does not occur in the bilayer leaflet interacting with the C-terminus, which has a more random distribution of lipids.

phosphates was similar in both leaflets of the bilayer. The density of the DPPE phosphates within 1 nm of FK1TMD was also lower than that of PIP2.

CD Spectroscopy. The secondary structure of FK1TMD reconstituted into saturated phospholipids with varying chain lengths was investigated using CD spectroscopy. FK1TMD was reconstituted at a lipid:protein ratio of 100:1 that resulted in the formation of bilayer structures for all lipids with the exception of DHPC, for which micellar structures were formed. To ensure CD spectra were acquired for all bilayer-forming lipids in the liquid crystalline phase, data were recorded at both 25 and 43 °C. For all bilayer-forming lipids, the CD spectra at 25 and 43 °C showed distinct minima at 208 and 222 nm with a maximum at 195 nm consistent with FK1TMD forming an α-helical structure as predicted (Figure 4). In contrast, the spectra of FK1TMD in DHPC micelles showed a less distinct minimum at 208 nm and reduced elipticity at 195 nm suggesting that additional secondary structures may contribute the observed CD spectra.

The quantitation of CD spectra of integral membrane proteins and peptides remains challenging because of the paucity of membrane protein structures in the basis sets employed during analysis, the scattering observed from the lipid vesicles (*42*, *43*), and other environmental factors (*44*). However, they still provide useful insights into changes in the secondary structure composition of proteins and peptides within (or associated with) the lipid bilayer. A quantitative analysis of the α-helical contribution to the CD spectra is given in Table 1. As expected, FK1TMD in bilayer-forming lipids is almost entirely α-helical. In the case of DPPC, this indicates that the secondary structure of FK1TMD remained invariant irrespective of whether the surrounding bilayer was in its liquid crystalline or gel phase. Interestingly, the α-helical contribution to the CD spectra in the bilayer-forming lipids appears not to vary as a function of bilayer thickness, suggesting that changes in bilayer thickness are accommodated by changes in the orientation of the TMD within the bilayer in agreement with the molecular dynamics studies. FK1TMD in DHPC micelles also revealed extensive α-helical structures, with more than 90% of the residues in a helical conformation at both temperatures. The analysis of FK1TMD in DHPC micelles at 43 °C indicated a small decrease in helical content compared to that observed at 25 °C, although the significance, if any, of this observation will require more detailed structural studies.

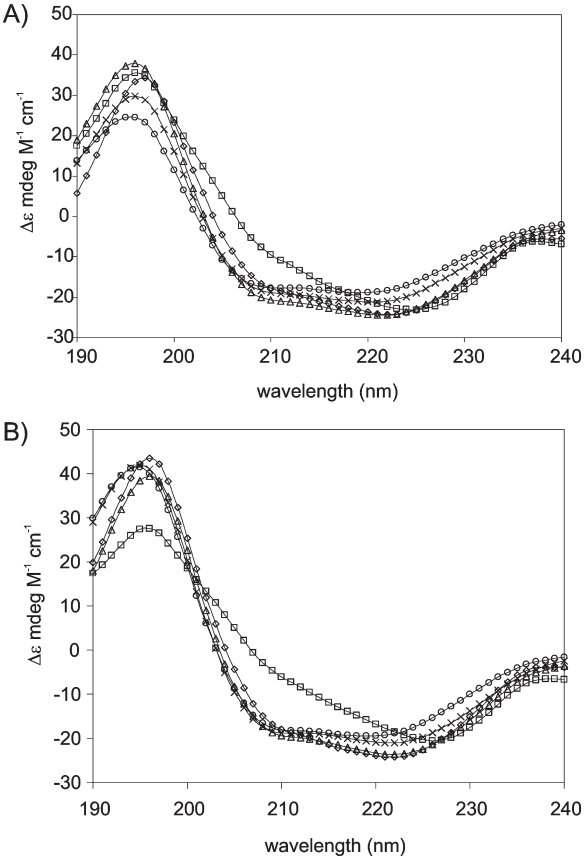

FIGURE 4: CD spectra of FK1TMD in SUVs of differing lipid chain lengths prepared by sonication at (A) 25 °C and (B) 43 °C: (□) C6, (○) C10, (×) C12, (△) C14, and (◇) C16. The final peptide concentration was 0.2 mg/mL. Each spectrum is an average of six recorded at a speed of 100 nm/min. The spectra display molar circular dichroism $\Delta\varepsilon$ (millidegrees per molar per centimeter) as a function of wavelength (nanometers).

DISCUSSION

In conclusion, we have used ATMD simulations to assess the stability of FK1TMD. Our simulations have shown that it is a stable α-helix in DPPC and DMPC bilayers in a TM orientation but partially unfolds when lying parallel to the plain of the bilayer, at the headgroup−water interface. The differences in

Table 1: α-Helical Content of the FK1TMD Peptide as a Function of Lipid Chain Length at 25 and 43 °C[a]

	25 °C		43 °C	
chain length	helical content (%)	nrmsd[b]	helical content (%)	nrmsd[b]
DHPC	98.7	0.086	90.7	0.120
DDPC	98.2	0.093	97.9	0.078
DLPC	99.6	0.093	99.0	0.068
DMPC	98.8	0.061	98.1	0.054
DPPC	97.4	0.137	97.5	0.069

[a]Helical content determined using the CONTIN/LL algorithm (*37*, *38*) with basis set 7 within Dichroweb (*39*, *40*). [b]The nrmsd (normalized root-mean-square deviation) defines the extent of agreement between the experimental CD spectrum and that derived during the analysis (*2*). Note this is not a measure of agreement between the CD spectra and the structures observed in the molecular dynamics simulations.

lipid tail length did not affect the stability of the helix. These results have been corroborated by CD measurements, which confirm that the helical content of the peptide remains invariant as a function of bilayer thickness. CGMD simulations of bilayer self-assembly confirm the preference for the TM orientation. The charged residues anchor both termini of FK1TMD in the headgroup region of the lipid bilayer. To further investigate the effect of lipid tails and headgroups on the membrane orientation and localization of FK1TMD, we performed CGMD simulations in three different lipid tails and also a mixture of headgroups that closely mimics the in vivo Golgi membrane composition. To the best of our knowledge, these are the most detailed CGMD simulations of the Golgi membrane reported to date. Our simulations predict the FK1TMD tilt angle to be sensitive to the composition of the surrounding lipid bilayer. Furthermore, we show that the N-terminal domain of the protein exhibits a marked propensity to interact with PIP2 lipids and may play a role in the formation of microdomains by inducing clustering of these lipids. A possible limitation of this study is that only the TM domain of the fukutin protein is considered; while we note that similar studies of isolated TM domains have previously been used to explore their membrane interactions, the inclusion of neighboring domains would provide additional insights into the dynamics of the functional protein (*30*, *41*).

In summary, our results provide evidence that the TM domain of fukutin is a stable helix, whose stability is not affected by the width of the local membrane. Rather, the protein responds to changes in bilayer thickness via its substantial mobility and ability to tilt within the bilayer. The changes observed in the tilt of the helix as a function of bilayer thickness have implications for how the protein may respond to the differing bilayer compositions found within the different intracellular compartments, with implications for protein packing and the formation of higher oligomeric structures as well as its preference for proteins to associate with lipid bilayers with distinct physical properties. These properties are the subject on ongoing investigations, with a view of discerning the involvement in the retention of fukutin and other ER/GA resident proteins. Finally, while some aspects of the Golgi membrane such as the full extent of lipid tail composition have not been explored here, our simulations of the complex Golgi membrane represent a key step toward linking in silico experiments with real biological systems.

ACKNOWLEDGMENT

S.K., D.A.H., and T.J.P. thank Phillip Stansfeld and Peter Tieleman for help with lipid parameters.

SUPPORTING INFORMATION AVAILABLE

Detailed description of the materials and methods and analysis via rmsd, secondary structure analysis, protein−lipid contacts, and radial distribution functions from simulations. This material is available free of charge via the Internet at http://pubs.acs.org.

REFERENCES

1. Martin-Rendon, E., and Blake, D. J. (2003) Protein glycosylation in disease: New insights into the congenital muscular dystrophies. *Trends Pharmacol. Sci. 24*, 178–183.
2. Torelli, S., Brown, S. C., Brockington, M., Dolatshad, N. F., Jimenez, C., Skordis, L., Feng, L. H., Merlini, L., Jones, D. H., Romero, N., Wewer, U., Voit, T., Sewry, C. A., Noguchi, S., Nishino, I., and Muntoni, F. (2005) Sub-cellular localisation of fukutin related protein in different cell lines and in the muscle patients with MDC1C and LGMD2I. *Neuromuscular Disord. 15*, 836–843.
3. Keramaris-Vrantsis, E., Lu, P. J., Doran, T., Zillmer, A., Ashar, J., Esapa, C. T., Benson, M. A., Blake, D. J., Rosenfeld, J., and Lu, Q. L. (2007) Fukutin-related protein localizes to the Golgi apparatus and mutations lead to mislocalization in muscle in vivo. *Muscle Nerve 36*, 455–465.
4. Matsumoto, H., Noguchi, S., Sugie, K., Ogawa, M., Murayama, K., Hayashi, Y. K., and Nishino, I. (2004) Subcellular localization of fukutin and fukutin-related protein in muscle cells. *J. Biochem. 135*, 709–712.
5. Lommel, M., Willer, T., and Strahl, S. (2008) POMT2, a key enzyme in Walker-Warburg syndrome: Somatic sPOMT2, but not testis specific POMT2, is crucial for mannosyltransferase activity in vivo. *Glycobiology 18*, 615–625.
6. Opat, A. S., van Vliet, C., and Gleeson, P. A. (2001) Trafficking and localisation of resident Golgi glycosylation enzymes. *Biochimie 83*, 763–773.
7. Gleeson, P. A. (1998) Targeting of proteins to the Golgi apparatus. *Histochem. Cell Biol. 109*, 517–532.
8. Pelham, H. R. B., and Munro, S. (1993) Sorting of membrane proteins in the secretory pathway. *Cell 75*, 603–605.
9. Esapa, C. T., McIlhinney, R. A., and Blake, D. J. (2005) Fukutin-related protein mutations that cause congenital muscular dystrophy result in ER-retention of the mutant protein in cultured cells. *Hum. Mol. Genet. 14*, 295–305.
10. Munro, S. (1998) Localization of proteins to the Golgi apparatus. *Trends Cell Biol. 8*, 11–15.
11. Rayner, J. C., and Pelham, H. R. B. (1997) Transmembrane domain-dependent sorting of proteins to the ER and plasma membrane in yeast. *EMBO J. 16*, 1832–1841.
12. Marius, P., Wright, J. N., Findlow, I. S., and Williamson, P. T. (2010) Expression and purification of the transmembrane domain of Fukutin-I for biophysical studies. *Protein Expression Purif. 72*, 107–112.
13. Marti-Renom, M. A., Stuart, A. C., Fiser, A., Sanchez, R., Melo, F., and Sali, A. (2000) Comparative protein structure modeling of genes and genomes. *Annu. Rev. Biophys. Biomol. Struct. 29*, 291–325.
14. Laskowski, R. A., Moss, D. S., and Thornton, J. M. (1993) Main-chain bond lengths and bond angles in protein structures. *J. Mol. Biol. 231*, 1049–1067.
15. Van der Spoel, D., Lindahl, E., Hess, B., Groenhof, G., Mark, A. E., and Berendsen, H. J. C. (2005) Gromacs: Fast, Flexible, and Free. *J. Comput. Chem. 26*, 1701–1718.
16. Berendsen, H. J. C., Vanderspoel, D., and Vandrunen, R. (1995) Gromacs: A Message-Passing Parallel Molecular-Dynamics Implementation. *Comput. Phys. Commun. 91*, 43–56.
17. Hess, B., Kutzner, C., van der Spoel, D., and Lindahl, E. (2008) GROMACS 4: Algorithms for highly efficient, load-balanced, and scalable molecular simulation. *J. Chem. Theory Comput. 4*, 435–447.
18. Schuler, L. D., Daura, X., and Van Gunsteren, W. F. (2001) An improved GROMOS96 force field for aliphatic hydrocarbons in the condensed phase. *J. Comput. Chem. 22*, 1205–1218.
19. Berger, O., Edholm, O., and Jahnig, F. (1997) Molecular dynamics simulations of a fluid bilayer of dipalmitoylphosphatidylcholine at full hydration, constant pressure, and constant temperature. *Biophys. J. 72*, 2002–2013.
20. Berendsen, H. J. C., Postma, J. P. M., van Gunsteren, W. F., and Hermans, J. (1981) in Intermolecular Forces, Reidel, Dordrecht, The Netherlands.
21. Hess, B. (2008) P-LINCS: A parallel linear constraint solver for molecular simulation. *J. Chem. Theory Comput. 4*, 116–122.
22. Miyamoto, S., and Kollman, P. A. (1992) Settle: An Analytical Version of the Shake and Rattle Algorithm for Rigid Water Models. *J. Comput. Chem. 13*, 952–962.

23. Bussi, G., Donadio, D., and Parrinello, M. (2007) Canonical sampling through velocity rescaling. *J. Chem. Phys. 126*, 014101.
24. Berendsen, H. J. C., Postma, J. P. M., Vangunsteren, W. F., Dinola, A., and Haak, J. R. (1984) Molecular-Dynamics with Coupling to an External Bath. *J. Chem. Phys. 81*, 3684–3690.
25. Essmann, U., Perera, L., Berkowitz, M. L., Darden, T., Lee, H., and Pedersen, L. G. (1995) A Smooth Particle Mesh Ewald Method. *J. Chem. Phys. 103*, 8577–8593.
26. Kabsch, W., and Sander, C. (1983) Dictionary of Protein Secondary Structure: Pattern-Recognition of Hydrogen-Bonded and Geometrical Features. *Biopolymers 22*, 2577–2637.
27. Humphrey, W., Dalke, A., and Schulten, K. (1996) VMD: Visual molecular dynamics. *J. Mol. Graphics 14*, 33–38.
28. Marrink, S. J., de Vries, A. H., and Mark, A. E. (2004) Coarse grained model for semiquantitative lipid simulations. *J. Phys. Chem. B 108*, 750–760.
29. Bond, P. J., and Sansom, M. S. (2006) Insertion and assembly of membrane proteins via simulation. *J. Am. Chem. Soc. 128*, 2697–2704.
30. Carpenter, T., Bond, P. J., Khalid, S., and Sansom, M. S. P. (2008) Self-assembly of a simple membrane protein: Coarse-grained molecular dynamics simulations of the influenza M2 channel. *Biophys. J. 95*, 3790–3801.
31. Lopez, C. A., Rzepiela, A. J., de Vries, A. H., Dijkhuizen, L., Hunenberger, P. H., and Marrink, S. J. (2009) Martini Coarse-Grained Force Field: Extension to Carbohydrates. *J. Chem. Theory Comput. 5*, 3195–3210.
32. Lins, R. D., and Hunenberger, P. H. (2005) A new GROMOS force field for hexopyranose-based carbohydrates. *J. Comput. Chem. 26*, 1400–1412.
33. Bond, P. J., Holyoake, J., Ivetac, A., Khalid, S., and Sansom, M. S. (2007) Coarse-grained molecular dynamics simulations of membrane proteins and peptides. *J. Struct. Biol. 157*, 593–605.
34. Bond, P. J., Wee, C. L., and Sansom, M. S. P. (2008) Coarse-Grained Molecular Dynamics Simulations of the Energetics of Helix Insertion into a Lipid Bilayer. *Biochemistry 47*, 11321–11331.
35. Marrink, S. J., Risselada, H. J., Yefimov, S., Tieleman, D. P., and de Vries, A. H. (2007) The MARTINI force field: Coarse grained model for biomolecular simulations. *J. Phys. Chem. B 111*, 7812–7824.
36. van Meer, G. (1998) Lipids of the Golgi membrane. *Trends Cell Biol. 8*, 29–33.
37. Provencher, S. W., and Glockner, J. (1981) Estimation of globular protein secondary structure from circular dichroism. *Biochemistry 20*, 33–37.
38. van Stokkum, I. H., Spoelder, H. J., Bloemendal, M., van Grondelle, R., and Groen, F. C. (1990) Estimation of protein secondary structure and error analysis from circular dichroism spectra. *Anal. Biochem. 191*, 110–118.
39. Whitmore, L., and Wallace, B. A. (2004) DICHROWEB, an online server for protein secondary structure analyses from circular dichroism spectroscopic data. *Nucleic Acids Res. 32*, W668–W673.
40. Whitmore, L., and Wallace, B. A. (2008) Protein secondary structure analyses from circular dichroism spectroscopy: Methods and reference databases. *Biopolymers 89*, 392–400.
41. Rouse, S. L., Carpenter, T., Stansfeld, P. J., and Sansom, M. S. P. (2009) Simulations of the BM2 Proton Channel Transmembrane Domain from Influenza Virus B. *Biochemistry 48*, 9949–9951.
42. Wallace, B. A., and Mao, D. (1984) Circular dichroism analyses of membrane proteins: An examination of differential light scattering and absorption flattening effects in large membrane vesicles and membrane sheets. *Anal. Biochem. 142*, 317–328.
43. Mao, D., and Wallace, B. A. (1984) Differential light scattering and absorption flattening optical effects are minimal in the circular dichroism spectra of small unilamellar vesicles. *Biochemistry 23*, 2667–2673.
44. Swords, N. A., and Wallace, B. A. (1993) Circular-dichroism analyses of membrane proteins: Examination of environmental effects on bacteriorhodopsin spectra. *Biochem. J. 289* (Part 1), 215–219.